



# Synthesis and electrochemical characterization of Cr-doped lithium-rich $\text{Li}_{1.2}\text{Ni}_{0.16}\text{Mn}_{0.56}\text{Co}_{0.08-x}\text{Cr}_x\text{O}_2$ cathodes

Umair Nisar<sup>1</sup> · Ruhul Amin<sup>2</sup> · Abdul Shakoor<sup>1</sup> · Rachid Essehli<sup>2</sup> · Siham Al-Qaradawi<sup>3</sup> · Ramazan Kahraman<sup>4</sup> · Ilias Belharouak<sup>5</sup>

Received: 28 May 2018 / Accepted: 25 September 2018 / Published online: 15 October 2018  
© Springer Nature Switzerland AG 2018

## Abstract

Lithium-rich layer oxide,  $\text{Li}_{1.2}\text{Ni}_{0.16}\text{Mn}_{0.56}\text{Co}_{0.08}\text{O}_2$  (NMC), is a potential cathode candidate for high-energy density batteries. Issues such as cycling stability, rate performance, and cost are yet to be overcome before successful commercialization of the material. Here, we report on the synthesis of Cr-doped lithium-rich phases  $\text{Li}_{1.2}\text{Ni}_{0.16}\text{Mn}_{0.56}\text{Co}_{0.08-x}\text{Cr}_x\text{O}_2$  (where  $x = 0.00, 0.01,$  and  $0.02$ ) (NMC-Cr) by the sol-gel technique. Cr is homogeneously distributed in the crystal structure evidence by elemental mapping measurements. The Cr-doped materials exhibit much better cycling stability with 100% capacity retention versus 44% for the undoped sample after 50 cycles. The Cr-doped samples show excellent electrochemical performance at higher C-rate in comparison with the undoped NMC. The latter shows rapid capacity fading from 220 to 50 mAh  $\text{g}^{-1}$  at the 0.1 to 1C rates, respectively. Moreover, the Cr-containing materials do not show significant signs of voltage fading during cycling owing to the stabilization of the crystal lattice by Cr. The electrochemical impedance spectroscopy measurements also indicate the stable cell resistance on cycling for the Cr-doped phases compared to the undoped phase.

**Keywords** Battery · Lithium-rich cathode · Layer structure · Impedance · Doped · Sol-gel

Umair Nisar and Ruhul Amin contributed equally to this work.

**Electronic supplementary material** The online version of this article (<https://doi.org/10.1007/s42247-018-0014-0>) contains supplementary material, which is available to authorized users.

✉ Ruhul Amin  
mdruhul@hbku.edu.qa

✉ Abdul Shakoor  
shakoor@qu.edu.qa

<sup>1</sup> Center for Advanced Materials (CAM), Qatar University, Doha, Qatar

<sup>2</sup> Qatar Environment and Energy Research Institute, Hamad Bin Khalifa University, Qatar Foundation, Doha, Qatar

<sup>3</sup> Department of Chemistry & Earth Sciences, College of Arts and Science, Qatar University, Doha, Qatar

<sup>4</sup> Department of Chemical Engineering, College of Engineering, Qatar University, Doha, Qatar

<sup>5</sup> Energy and Transportation Science Division, Oak Ridge National Laboratory, Oak Ridge, TN, USA

## 1 Introduction

Due to limited fossil fuel reserves and environmental concerns, the world is investing in renewable energy sources such as solar and wind energies. However, the energy supplied by these energy sources is intermittent, and therefore, efficient energy storage systems (ESS) need to be developed which can store the excess amount of energy from these renewable sources and supply when needed [1–4]. Among various existing ESS, lithium-ion batteries are considered among the best choices due to their high operating voltage, good calendar life, and high energy and power densities [5–9]. Nonetheless, the energy density of the current lithium-ion battery technology is not enough to fulfill future energy storage demands; therefore, new battery chemistries need to be developed having higher operating voltages and higher specific capacities [6, 10, 11]. The cost, environmental, and safety concerns should also be taken into consideration for future applications [1, 3, 7, 8].

During the last two decades, several different cathode materials have been developed and employed successfully in commercial lithium-ion batteries which include  $\text{LiCoO}_2$ ,

$\text{LiMn}_2\text{O}_4$ ,  $\text{LiNi}_{0.5}\text{Mn}_{1.5}\text{O}_4$ ,  $\text{LiNi}_{1/3}\text{Mn}_{1/3}\text{Co}_{1/3}\text{O}_2$ ,  $\text{LiNi}_{0.8}\text{Co}_{0.15}\text{Al}_{0.05}\text{O}_2$ , and  $\text{LiFePO}_4$  [12–22]. However, the available capacities for these materials already reached their practical limits; therefore, a new class of cathode materials needs to be developed with higher specific capacities ( $> 200 \text{ mAh g}^{-1}$ ) with lower cost and enhanced safety [23, 24].

More recently, lithium-rich layered oxide ( $x\text{Li}_2\text{MnO}_3 \cdot (1-x)\text{LiMO}_2$  ( $M = \text{Mn, Ni, Co, Fe, etc.}$ )) materials have attracted considerable attention as a high-energy density cathode material for lithium-ion batteries owing to their high specific capacities ( $> 250 \text{ mAh g}^{-1}$ ) and high operating voltages ( $> 3.6 \text{ V}$ ) [23–28]. Unfortunately, these materials are prone to rapid voltage and capacity decay during cycling which has seriously hindered the development and commercialization of these materials in practical batteries. Other scientific challenges related to this class of materials which include poor rate capabilities, low initial coulombic efficiency, structural instability, and safety concerns also are needed to be paid great scientific attention before their commercialization [29–34]. To mitigate these problems, various strategies have been adopted such as doping on Mn, Ni, or Co sites with different transition metals [35–43], tailoring the particles morphology [22, 44–46] and surface modification by using different materials [47–51]. Among these approaches, doping in the lattice position is considered one of the most acceptable techniques to improve the performance of the material in terms of longer cyclability and rate capability through improvement of structural stability and transport properties. A variety of transition metal dopants such as Fe, Zr, Co, Mg, Cr, Zn, Ti, Mo, and Ru [36, 38, 40–42, 52–55] have been investigated in different cathode materials. Co is the expensive component in the NMC layer structure materials compare to Ni or Mn.  $\text{Cr}^{3+}$  (ionic radius 0.62 Å) is a suitable dopant for substituting the  $\text{Co}^{3+}$  (ionic radius 0.60 Å) since they have similar ionic radius and valent state. It may not alter the electronic defect structure of the materials and is not even required as the transport properties of layer structure materials that are relatively high compared to other systems. Several studies have shown also the improvement in the performance electrochemical of different cathode material with Cr doping [39, 40, 56–58]. However, Cr doping may help to increase the structural and interfacial stability of the NMC cathode.

In this study,  $\text{Li}_{1.2}\text{Ni}_{0.16}\text{Mn}_{0.56}\text{Co}_{0.08-x}\text{Cr}_x\text{O}_2$  (where  $x = 0.00, 0.01, \text{ and } 0.02$ ) (MNC-Cr) have been synthesized by sol-gel synthesis. The synthesized materials have been characterized using X-ray diffraction (XRD), X-ray photoelectron spectroscopy (XPS), scanning electron microscopy (SEM), electrochemical charge/discharge, and electrochemical impedance spectroscopy (EIS). The Cr-doped samples show improvement in voltage fading, better rate capability, and better capacity retention during cycling.

## 2 Experimental

### 2.1 Materials preparation

$\text{Li}_{1.2}\text{Ni}_{0.16}\text{Mn}_{0.56}\text{Co}_{0.08-x}\text{Cr}_x\text{O}_2$  (where  $x = 0.00, 0.01, \text{ and } 0.02$ ) (MNC-Cr) were prepared via sol-gel method using lithium, manganese, nickel, cobalt, and chromium acetates (Sigma-Aldrich) in the molar ratio 1.2:0.16:0.56:0.08, respectively. The precursors were dissolved in 100 ml of distilled water in the presence of citric acid. The molar ratio total-ions/citric-acid was fixed at 1:1. The resulting solution was kept at  $70 \text{ }^\circ\text{C}$  until a transparent gel was obtained. The gel was dried in an oven at  $120 \text{ }^\circ\text{C}$ . The dried gel was crushed and grinded using agate mortar to homogenously mix the precursor and finally calcined at  $900 \text{ }^\circ\text{C}$  for 12 h in the air. The detailed experimental procedure is shown in the Fig. 1.

### 2.2 Physical characterization

The powder X-ray diffraction (XRD) measurements were performed to identify the phase purity of the synthesized materials in the Bragg-Brentano reflection geometry between  $10$  and  $80^\circ$  ( $2\theta$  value) using a Bruker D8 diffractometer equipped with a 1.6-kW sealed X-ray tube source (Cu-K $\alpha$  radiation) and a Vantec2000 2D detector. The particle morphology was investigated by field emission scanning electron microscopy (FE-SEM, Nova). In order to investigate the oxidation states of transition metals, the particles were investigated with X-ray photoelectron spectroscopy (XPS) (Thermo-Scientific-Sigma Probe).

### 2.3 Electrode fabrication

The positive electrode was fabricated by casting a slurry composed of 80 wt.% (MNC or MNC-Cr) active material, 10 wt.% conductive carbon (Super-P), and 10 wt.% poly(vinylidene fluoride) binder in 1-methyl-2-pyrrolidone (NMP) on an aluminum foil using doctor blade. The electrode was dried at  $80 \text{ }^\circ\text{C}$  to remove NMP and then vacuum-dried at  $120 \text{ }^\circ\text{C}$  to remove traces of moisture. The electrode was cut into electrodes of 14 mm diameter and was  $30 \text{ }\mu\text{m}$  thick.

### 2.4 Electrochemical measurements

Electrochemical measurements were carried out using 2032-type coin cells assembled with doped and undoped  $\text{Li}_{1.2}\text{Ni}_{0.16}\text{Mn}_{0.56}\text{Co}_{0.08-x}\text{Cr}_x\text{O}_2$  (where  $x = 0.00, 0.01, \text{ and } 0.02$ ) in an Ar-filled glove box. Lithium foil was used as the negative electrode. The electrolyte was made of 1 M  $\text{LiPF}_6$  dissolved in a solvent mixture of ethylene carbonate (EC) and dimethyl carbonate (DMC) (1:1 by v/v). Galvanostatic charge/discharge tests were performed at  $25 \text{ }^\circ\text{C}$  using Solartron battery cycler (1470E). The cells were tested under different C-

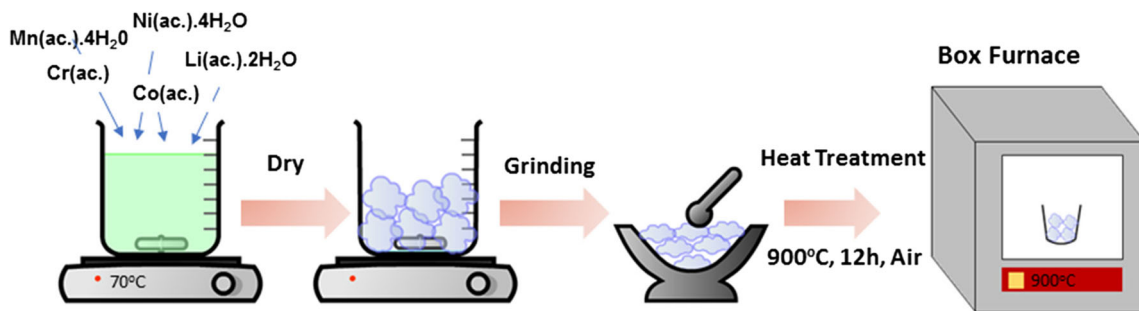


Fig. 1 Schematic figure showing the experimental procedure for making NMC cathode

rate conditions to check the rate performance of the materials. The cells were always charged and discharge at the same current at different C-rate.

The electrochemical impedance spectroscopy (EIS) measurements were performed at three different states of charge and discharge using Solartron battery cyclers (1470E). First, the cell was charged or discharged at a specific state of charge and kept in open circuit condition for at least 2 hours to reach a steady-state voltage condition. Then the EIS measurement was performed in the frequency range from 2 MeGHz to 5 mHz with applied AC amplitude of 10 mV.

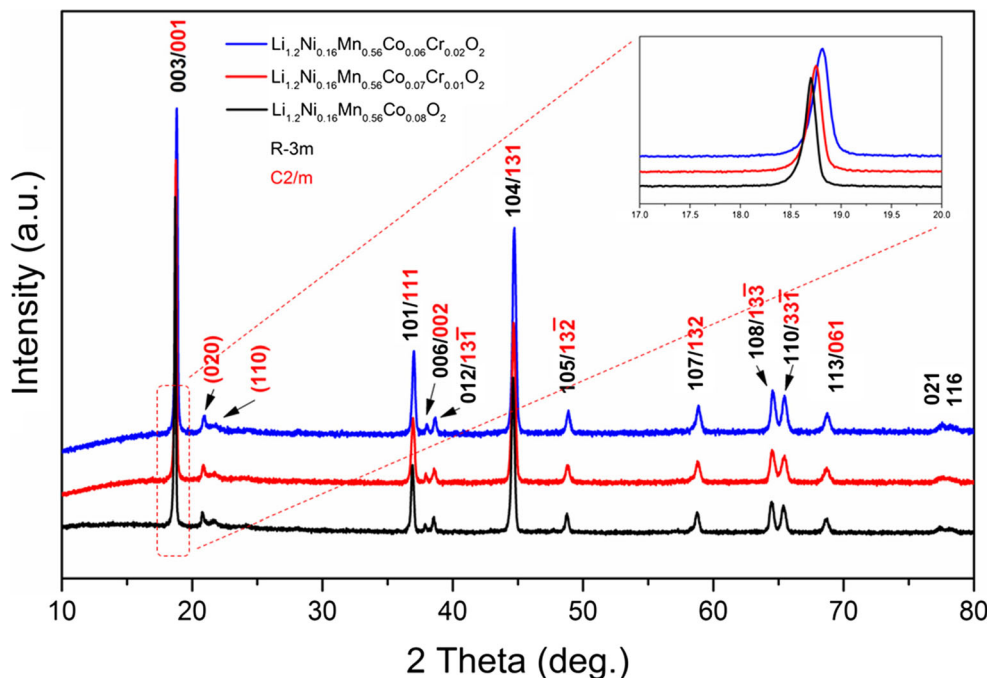
### 3 Results and discussion

Figure 2 compares the X-ray diffraction (XRD) patterns of undoped and Cr-doped  $\text{Li}_{1.2}\text{Ni}_{0.16}\text{Mn}_{0.56}\text{Co}_{0.08-x}\text{Cr}_x\text{O}_2$  (where  $x = 0.00, 0.01, \text{ and } 0.02$ ) which indicate impurity-free phases with highly crystalline structure. Most of the peaks can be indexed based on the R-3m space group except

for the peaks between 20 and 30°, which can only be indexed based on the monoclinic (C2/m) space group. On this basis, the material can be characterized as a combination of two phases, namely, a trigonal R-3m phase and a monoclinic C2/m phase which is consistent with the XRD data reported by Jarvis et al. [59]. However, all the observed peaks can also be indexed based on the C2/m structure [34]. It is interesting to note that the characteristic diffraction peaks shifted towards higher 2θ values due to the increase of the Cr content in the phase (inset of Fig. 2) which indicates that  $\text{Cr}^{3+}$  doped the crystalline lattice rather than being segregated as an impurity phase. Though the ionic radius of  $\text{Cr}^{3+}$  (ionic radius  $0.62\text{Å}$ ) and  $\text{Co}^{3+}$  (ionic radius  $0.60\text{Å}$ ) is almost same, the small peaks shifting of 2θ towards higher values might be originated due to differences per distribution function of Co and Cr.

The lattice parameters of pristine and Cr-doped samples were evaluated by X-ray Rietveld refinement analysis. All the observed peaks were matched with the calculated peak position. Figure 3 shows as a representative of

Fig. 2 XRD patterns for  $\text{Li}_{1.2}\text{Ni}_{0.16}\text{Mn}_{0.56}\text{Co}_{0.08-x}\text{Cr}_x\text{O}_2$  (where  $x = 0.00, 0.01, \text{ and } 0.02$ ). Inset shows the zoomed area 17–20°



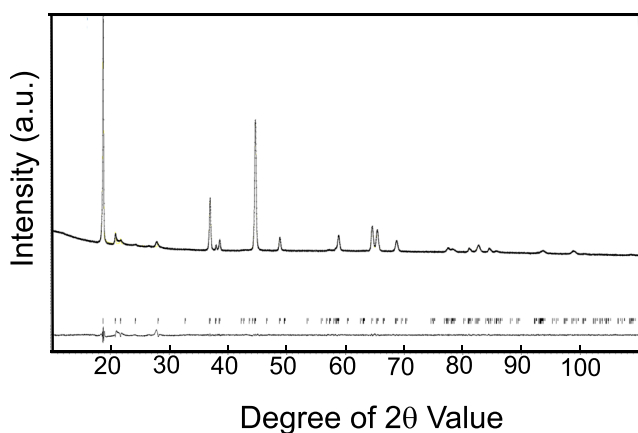


**Fig. 3** Displays the final observed and calculated plots for X-ray Rietveld refinement of  $\text{Li}_{1.2}\text{Ni}_{0.16}\text{Mn}_{0.56}\text{Co}_{0.06}\text{Cr}_{0.02}\text{O}_2$

$\text{Li}_{1.2}\text{Ni}_{0.16}\text{Mn}_{0.56}\text{Co}_{0.06}\text{Cr}_{0.02}\text{O}_2$  composition. Other samples also show similar patterns as presented in the supplementary information (Fig. S1). The calculated cell parameters were displayed in the Table 1 for the three samples. It is discernible from Table 1 that the lattice parameters and cell volume were increased slightly compared to the pristine sample  $\text{Li}_{1.2}\text{Ni}_{0.16}\text{Mn}_{0.56}\text{Co}_{0.08}\text{O}_2$  as the ionic radius of  $\text{Co}^{3+}$  is slightly smaller than that of  $\text{Cr}^{3+}$ . The small amount of Mn might also be substituted by Cr. The obtained lattice parameters reveal that the Cr is doped on the lattice position rather than segregated as an impurity content.

The SEM images of the  $\text{Li}_{1.2}\text{Ni}_{0.16}\text{Mn}_{0.56}\text{Co}_{0.08-x}\text{Cr}_x\text{O}_2$  (where  $x = 0.00, 0.01, \text{ and } 0.02$ ) samples heat-treated at  $900\text{ }^\circ\text{C}$  are displayed in Fig. 4. The samples are composed of numerous crystallites with a diameter of  $\sim 200\text{--}700\text{ nm}$ . However, the Cr-doped samples exhibit lower average particle sizes than the undoped sample (Fig. 4a). The particles sizes were become smaller with increasing the Cr-content as shown in Fig. 4c, e. All particles had similar rock-like grain morphology. A closer examination led us to observe that the particle aggregation increased with Cr despite of the formation of lower particle sizes as clearly visible in Fig. 4c, e. It is our hypothesis that a small amount of doped Cr-ions may not form continuous grain

**Table 1** Cell parameters of  $\text{Li}_{1.2}\text{Mn}_{0.56}\text{Ni}_{0.16}\text{Co}_{0.08-x}\text{Cr}_x\text{O}_2$

	$\text{Li}_{1.2}\text{Mn}_{0.56}\text{Ni}_{0.16}\text{Co}_{0.08}\text{O}_2$	$\text{Li}_{1.2}\text{Mn}_{0.56}\text{Ni}_{0.16}\text{Co}_{0.07}\text{Cr}_{0.01}\text{O}_2$	$\text{Li}_{1.2}\text{Mn}_{0.56}\text{Ni}_{0.16}\text{Co}_{0.06}\text{Cr}_{0.02}\text{O}_2$
a (Å)	4.9529(2)	4.9542(3)	4.9541(3)
b (Å)	8.5538(3)	8.5570(5)	8.5587(5)
c (Å)	5.0311(2)	5.0280(3)	5.0291(3)
$\alpha$ (°)	90	90	90
$\beta$ (°)	109.246(4)	109.189(5)	109.193(5)
$\gamma$ (°)	90	90	90
V (Å <sup>3</sup> )	201.237(16)	201.31(2)	201.38(2)

boundary phases in the  $\text{Li}_{1.2}\text{Ni}_{0.16}\text{Mn}_{0.56}\text{Co}_{0.08-x}\text{Cr}_x\text{O}_2$  particles. As a result, there could be no enhanced mass diffusion transport at grain boundaries.

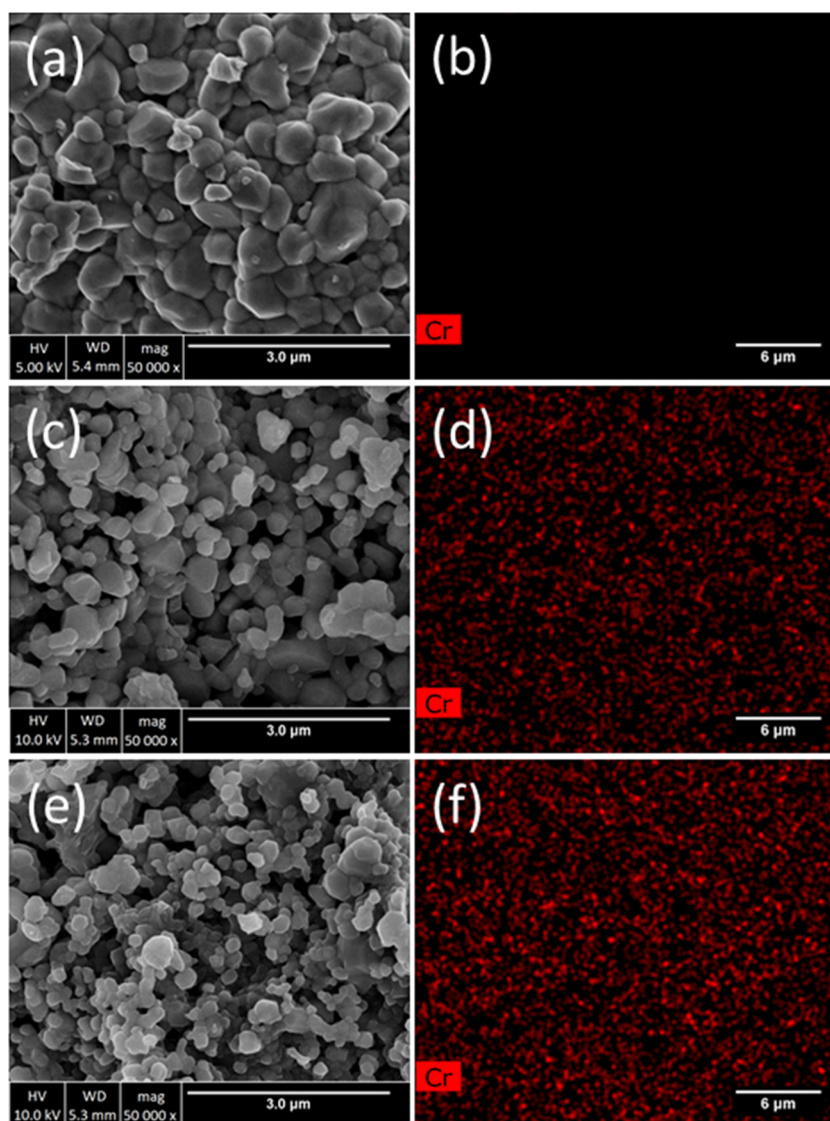
In this case, the scenario of Cr-doping does not promote grain growth of  $\text{Li}_{1.2}\text{Ni}_{0.16}\text{Mn}_{0.56}\text{Co}_{0.08-x}\text{Cr}_x\text{O}_2$ . It should be noted that the well-crystallized and small particles will help improve the rate performance and overall electrochemical properties of the cathode. In addition, the elemental mapping clearly shows that the Cr is homogeneously distributed in the grains (Fig. 4b–f) rather than being agglomerated or segregated heterogeneously.

The compositional studies of the synthesized materials,  $\text{Li}_{1.2}\text{Ni}_{0.16}\text{Mn}_{0.56}\text{Co}_{0.08-x}\text{Cr}_x\text{O}_2$  (where  $x = 0.00, 0.01, \text{ and } 0.02$ ), were also carried out by XPS measurement for evaluation of their phase purity. The XPS survey scans of the undoped and Cr-doped samples, heat-treated at  $900\text{ }^\circ\text{C}$ , are displayed in the supplementary information (Fig. S2) which reveals desired spectral lines of the Mn, Ni, Co, O, and Cr elements in the materials. The high-resolution XPS elemental spectra were deconvoluted, and plots are shown in Fig. 5, and binding energy of individual element is given in Table 2 and compared with the standard literature data.

The binding energies of Mn  $2p_{1/2}$  and Mn  $2p_{3/2}$  are around  $642.8\text{ eV} \pm 0.09$  and  $654.2 \pm 0.32$  (Fig. 5a–c), respectively, which are consistent with the value reported for  $\text{Mn}^{4+}$  in  $\text{MnO}_2$  [60, 61]. Two satellite peaks next to Mn  $2p_{1/2}$  and Mn  $2p_{3/2}$  are also observed in all three compositions. The binding energies for Ni  $2p_{1/2}$  and Ni  $2p_{3/2}$  are around  $872.77 \pm 0.07\text{ eV}$  and  $854.93\text{ eV} \pm 0.29$  (Fig. 5c, d, f), respectively, which corresponds to  $\text{Ni}^{2+}$  [60, 61]. Three satellite peaks are observed for Ni in all three samples. Furthermore, Fig. 5g–i shows that the binding energies for Co  $2p_{1/2}$  and Co  $2p_{3/2}$  are around  $795.4 \pm 0.27$  and  $780.45\text{ eV} \pm 0.27$  with the minor satellite peaks also present. The binding energies for Co 2p are consistent with  $\text{Co}^{3+}$  [60, 61]. The binding energies for Mn 2p, Ni 2p, and Co 2p slightly decrease with increasing the amount of Cr in the samples which indicate structural integrity of Cr in the synthesized phases. Figure 5j shows that there is no peak present for Cr in  $\text{Li}_{1.2}\text{Ni}_{0.16}\text{Mn}_{0.56}\text{Co}_{0.08}\text{O}_2$  which reveals the absence of Cr in this sample. The binding energies for Cr  $2p_{1/2}$  and Cr  $2p_{3/2}$  in  $\text{Li}_{1.2}\text{Ni}_{0.16}\text{Mn}_{0.56}\text{Co}_{0.07}\text{Cr}_{0.01}\text{O}_2$  and  $\text{Li}_{1.2}\text{Ni}_{0.16}\text{Mn}_{0.56}\text{Co}_{0.06}\text{Cr}_{0.02}\text{O}_2$  are at around  $588.17 \pm 0.13\text{ eV}$  and  $579.27 \pm 0.06$ , respectively, as shown in Fig. 5k, l. The binding energies for Cr 2p slightly increase with the amount of Cr in the samples as shown in Fig. 5k, l, which indicates lattice doping of Cr rather than segregated as impurity phases.

The voltage profile versus capacity of the undoped and doped  $\text{Li}_{1.2}\text{Ni}_{0.16}\text{Mn}_{0.56}\text{Co}_{0.08-x}\text{Cr}_x\text{O}_2$  (where  $x = 0.00, 0.01, \text{ and } 0.02$ ) are displayed in Fig. 6 under the charge and discharge at the C/5 rate. The cells were charged at a high-voltage up to 4.7 V and discharged down to 2 V. We can clearly observe from Fig. 6a that there was rapid

**Fig. 4** SEM and elemental mapping micrographs of  $\text{Li}_{1.2}\text{Ni}_{0.16}\text{Mn}_{0.56}\text{Co}_{0.08-x}\text{Cr}_x\text{O}_2$  (where  $x = 0.00, 0.01, \text{ and } 0.02$ ) heat-treated at  $900\text{ }^\circ\text{C}$  for 12 h. **a, b** Undoped. **c, d** Doped ( $x = 0.01$ ). **e, f** Doped ( $x = 0.02$ )



voltage decay and capacity fading for the undoped sample during discharged, whereas the stability of voltage and capacity increased with increasing the amount of Cr (Fig. 6b, c). Cr-doping has enhanced the structural stability of the solid solution, and hence, played a crucial role in improving the electrochemical performance of the material. In addition, the Cr-doped samples exhibited higher discharge capacities compared to the undoped sample. The reason could be due to the favorable interfacial kinetics at the electrode/electrolyte interfaces and enhanced electronic and ionic transport properties in the active particles at the relatively high C-rate.

Both doped and undoped  $\text{Li}_{1.2}\text{Ni}_{0.16}\text{Mn}_{0.56}\text{Co}_{0.08-x}\text{Cr}_x\text{O}_2$  (where  $x = 0.00, 0.01, \text{ and } 0.02$ ) materials showed relatively comparable capacities at lower C-rates. The undoped MNC delivered a specific capacity around  $220\text{ mAh g}^{-1}$  at the C/10 rate, whereas the Cr-doped NMC samples,  $x = 0.01$  and  $x = 0.02$ , delivered 195 and

$200\text{ mAh g}^{-1}$ , respectively, under the same C-rate. It should be noted that in the layer structure materials, Ni is treated as an electrochemical active species, while Mn and Co are inactive when cycled between 2.5 V and 4.2 V vs  $\text{Li}^+/\text{Li}$ . On the other hand, when charged up to 4.6 V  $\text{Co}^{3+}$  to  $\text{Co}^{4+}$ , oxidation occurs without any anionic redox activity [62–65]. In addition,  $\text{Co}^{3+}$  in the system helps to prevent the migration of  $\text{Ni}^{2+}$  to the layer at lithium position. The Cr doped might prevent the oxidation of  $\text{Co}^{3+}$  to  $\text{Co}^{4+}$  and might also not protect the migration of  $\text{Ni}^{2+}$  to the layer at lithium position. As a result, undoped samples exhibit higher capacity at lower cycling rate compared to Cr-doped samples. However, at higher cycling rates, capacity fading was very rapid for the undoped sample compared to that for the doped samples. It is clearly discernible from Fig. 7 that at the 1C-rate, the undoped sample showed a capacity around  $50\text{ mAh g}^{-1}$ , whereas the doped NMC-Cr ( $x = 0.02$ ) showed a capacity around  $150\text{ mAh g}^{-1}$ .

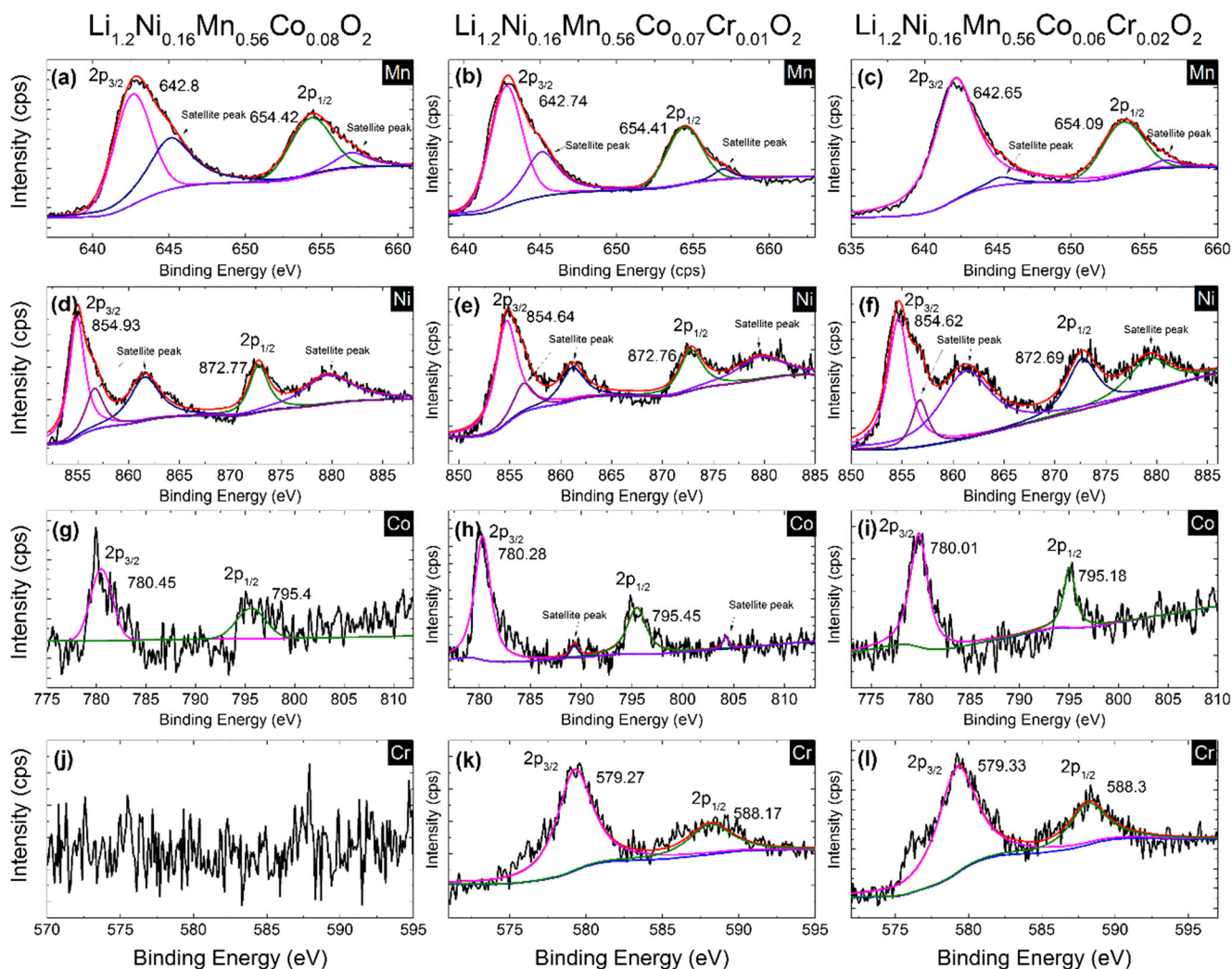


**Fig. 5** XPS spectra of  $\text{Li}_{1.2}\text{Ni}_{0.16}\text{Mn}_{0.56}\text{Co}_{0.08-x}\text{Cr}_x\text{O}_2$  (where  $x = 0.00, 0.01,$  and  $0.02$ ), separately showing the binding energy of Mn, Ni, Co, and Cr in the three different compositions. **a, d, g, j** Undoped phase ( $x = 0.00$ ). **b, e, h, k** Cr-doped phase ( $x = 0.01$ ). **c, f, i, l** C-doped phase ( $x = 0.02$ )

Moreover, the cycling under increasing rates from 0.1C to 1C demonstrates that the Cr-doped sample ( $x = 0.02$ ) exhibited a capacity retention of 75%, whereas the undoped sample displayed only 22% capacity retention. Figure 7 may also suggest that at higher C-rates, the performance limiting factor may either be slow phase boundary kinetics, ionic diffusivity, or increase charge transfer resistance at the electrode/electrolyte interface for the undoped material.

This will further be discussed in the section dedicated to the electrochemical impedance spectroscopy later. Fig. S3 shows the poor rate capability performance of  $\text{Li}_{1.2}\text{Ni}_{0.16}\text{Mn}_{0.56}\text{Co}_{0.05}\text{Cr}_{0.03}\text{O}_2$ .

Figure 8 compares the cycling performance of the undoped and Cr-doped  $\text{Li}_{1.2}\text{Ni}_{0.16}\text{Mn}_{0.56}\text{Co}_{0.08-x}\text{Cr}_x\text{O}_2$  (where  $x = 0.00, 0.01,$  and  $0.02$ ). The cell was charged at the C/2 rate and discharged at the same rate over 50

**Table 2** Binding energies for Mn, Ni, Co, and Cr in different samples

Composition	Mn		Ni		Co		Cr	
	2p <sub>3/2</sub>	2p <sub>1/2</sub>	2p <sub>3/2</sub>	2p <sub>1/2</sub>	2p <sub>3/2</sub>	2p <sub>1/2</sub>	2p <sub>3/2</sub>	2p <sub>1/2</sub>
$\text{Li}_{1.2}\text{Ni}_{0.16}\text{Mn}_{0.56}\text{Co}_{0.08}\text{O}_2$	642.80	654.42	854.93	872.78	780.45	795.46	–	–
$\text{Li}_{1.2}\text{Ni}_{0.16}\text{Mn}_{0.56}\text{Co}_{0.07}\text{Cr}_{0.01}\text{O}_2$	642.74	654.41	854.68	872.76	780.28	795.5	579.27	588.17
$\text{Li}_{1.2}\text{Ni}_{0.16}\text{Mn}_{0.56}\text{Co}_{0.06}\text{Cr}_{0.02}\text{O}_2$	642.65	654.09	854.62	872.69	780.01	795.18	579.33	588.30
Reference [60]	642.60	642.60	855.00	872.30	780.30	795.20	–	–

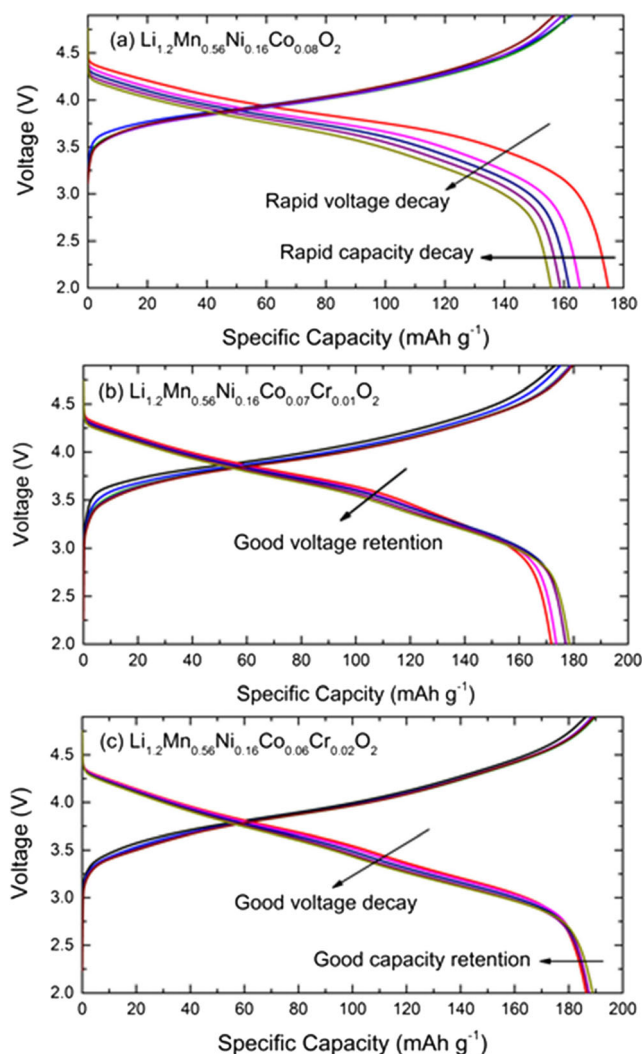


**Fig. 6** Galvanostatic cycling profile of lithium-rich **a** undoped and **b, c** Cr-doped  $\text{Li}_{1.2}\text{Ni}_{0.16}\text{Mn}_{0.56}\text{Co}_{0.08-x}\text{Cr}_x\text{O}_2$  (where  $x = 0.00, 0.01,$  and  $0.02$ ). The cells were charged and discharged at  $C/5$ -rate

cycles. It is seen from Fig. 8 that the capacity of the doped sample gradually increased with cycling and that of the undoped sample decreased rapidly on cycling. The

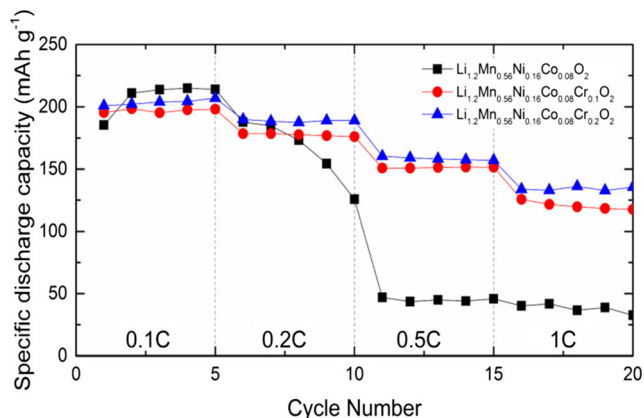


**Fig. 7** Rate capability of lithium-rich undoped and Cr-doped  $\text{Li}_{1.2}\text{Ni}_{0.16}\text{Mn}_{0.56}\text{Co}_{0.08-x}\text{Cr}_x\text{O}_2$  (where  $x = 0.00, 0.01,$  and  $0.02$ )

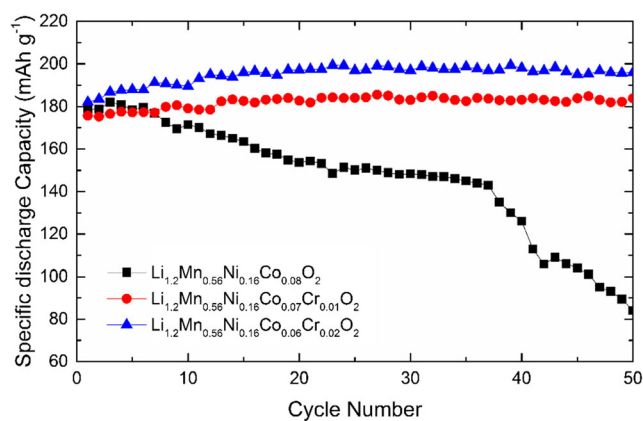
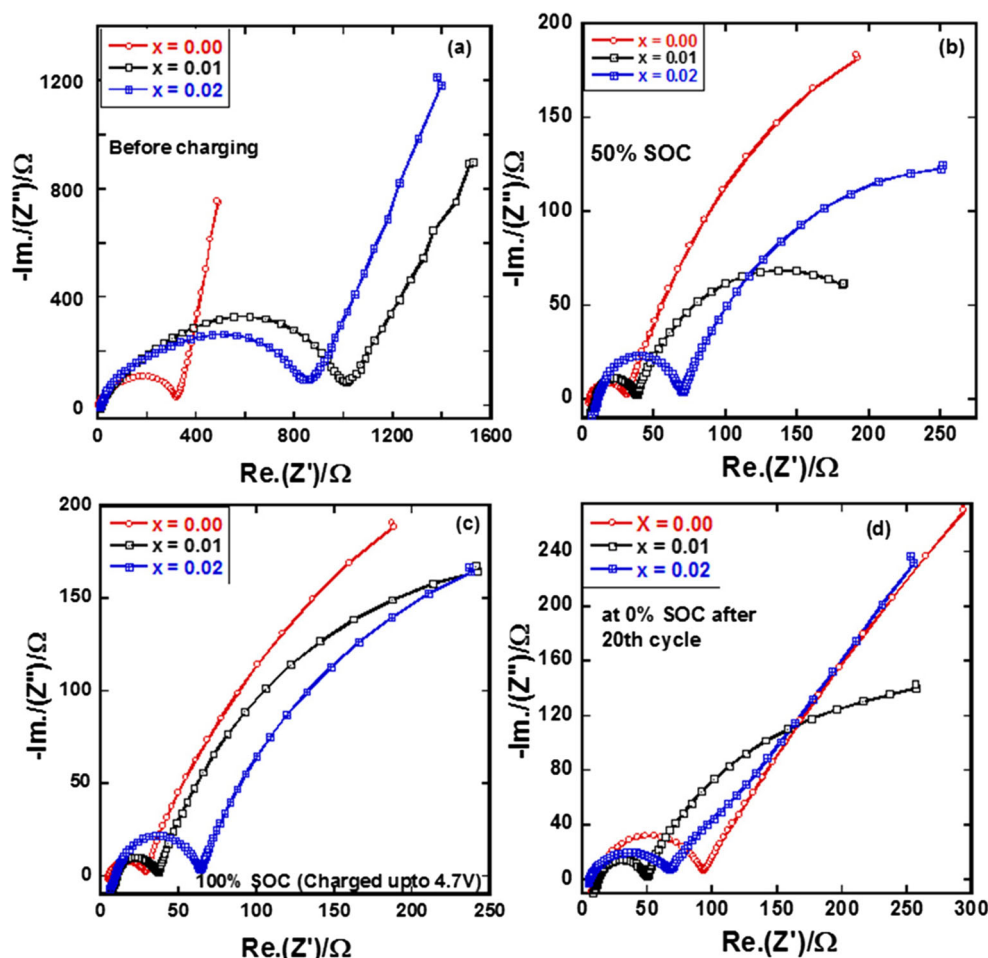


**Fig. 8** Discharge capacity of lithium-rich undoped and Cr-doped  $\text{Li}_{1.2}\text{Ni}_{0.16}\text{Mn}_{0.56}\text{Co}_{0.08-x}\text{Cr}_x\text{O}_2$  (where  $x = 0.00, 0.01,$  and  $0.02$ ) samples as a function of cycle number. All cells were charged and discharged at the  $0.2C$  rate

reason for the capacity enhancement is not clearly understood. However, as the particles are initially agglomerated (SEM micrograph in Fig. 4c, e), the particle surfaces are not fully exposed to the electrolyte which might be relaxed with subsequent cycling. On the other hand, Cr doping provided the structural stability that is needed for the improved cycling, unlike the undoped sample that had quick capacity fading with cycling. Nonetheless, the cyclability of the Cr-doped  $\text{Li}_{1.2}\text{Ni}_{0.16}\text{Mn}_{0.56}\text{Co}_{0.08-x}\text{Cr}_x\text{O}_2$  (where  $x = 0.00, 0.01,$  and  $0.02$ ) exhibited excellent electrochemical performance at the  $C/2$  rate for the first 50 cycles. The discharge capacity of the doped sample reached around  $200 \text{ mAh g}^{-1}$  after 50 cycles, whereas the capacity of the undoped sample was only 56% of its initial capacity.

To understand the differences in the electrochemical properties of Cr-doped and undoped  $\text{Li}_{1.2}\text{Ni}_{0.16}\text{Mn}_{0.56}\text{Co}_{0.08-x}\text{Cr}_x\text{O}_2$  (where  $x = 0.00, 0.01,$  and  $0.02$ ), we performed electrochemical impedance spectroscopy (EIS) measurements at three different states of charge (SOC) with lithium concentration intervals of 0%, 50%, and 100% SOC. Figure 9a compares the impedance spectra measured before the cycling of the cells. Initially, the undoped sample exhibited lower cell resistance compared to the doped samples. Figure 9b, c display the EIS spectra at 50% and 100% SOC (the cells were charged up to 4.7 V). One can observe from Fig. 9a, b, and c that the overall cell impedances decreased at 50% and 100% SOC. In this case, the trend was that the doped samples still exhibited higher cell impedances compared to the undoped sample. However, after several cycles, the trend was that the impedance of the undoped sample increased and kept increasing on further cycling compared to the Cr-doped samples (Fig. 9d). It should also be noted that capacity of the undoped sample decreased rapidly on cycling (Fig. 6) which is consistent with the results observed in the impedance measurements.

**Fig. 9** Impedance spectra of lithium-rich undoped and Cr-doped  $\text{Li}_{1.2}\text{Ni}_{0.16}\text{Mn}_{0.56}\text{Co}_{0.08-x}\text{Cr}_x\text{O}_2$  (where  $x = 0.00, 0.01,$  and  $0.02$ ) measured at three states of charge (SOC) at the first cycle at 0.0% (a) (before charging), 50% (b), and 100% (c) SOC (cell charged up to 4.7 V) and at the 20th cycle at 0.0% (d) (before charging)



## 4 Conclusions

The Li-rich layered Cr-doped oxide  $\text{Li}_{1.2}\text{Ni}_{0.16}\text{Mn}_{0.56}\text{Co}_{0.08-x}\text{Cr}_x\text{O}_2$  (where  $x = 0.00, 0.01,$  and  $0.02$ ) (NMC-Cr) were synthesized by the sol-gel process. XRD, XPS, and SEM measurements confirmed the purity of the crystalline phases with the morphology of rock-like grains and ensured the homogeneous distribution of Cr in the doped samples. The undoped material ( $x = 0.00$ ) exhibits rapid capacity fade on cycling and unsatisfactory rate capability. The rapid voltage fade is associated with the increase of the cell impedance on cycling. However, the Cr-doped phase ( $x = 0.02$ ) exhibits excellent rate capability and no capacity fade during 50 cycles which makes this material a potential alternative cathode suitable for powering electric vehicles, grid-level storage, and portable consumer products. The total cell resistance and interfacial charge transfer resistance are stable on cycling for the Cr-doped phases compared to those for the undoped phase. The Cr-doping strategy is effective in improving the structural stability of the NMC materials and hence the electrochemical performances.

## References

1. J.-M. Tarascon, Key challenges in future Li-battery research. *Philos Trans A Math Phys Eng Sci* **368**, 3227–3241 (2010). <https://doi.org/10.1098/rsta.2010.0112>
2. N. Nitta, F. Wu, J.T. Lee, G. Yushin, Li-ion battery materials: present and future. *Mater Today* **18**, 252–264 (2015). <https://doi.org/10.1016/j.mattod.2014.10.040>
3. S. Whittingham, Materials challenges facing electrical energy storage, (2008) 411–419. <http://www.ftconferences.com/userfiles/file/WhittinghamStanWhitepaper.pdf>
4. D. Larcher, J.-M. Tarascon, Towards greener and more sustainable batteries for electrical energy storage. *Nat. Chem* **7**, 19–29 (2015). <https://doi.org/10.1038/nchem.2085>
5. J.M. Tarascon, M. Armand, Issues and challenges facing rechargeable lithium batteries. *Nature* **414**, 359–367 (2001). <https://doi.org/10.1038/35104644>
6. A. Kraysberg, Y. Ein-Eli, A. Kraysberg, Y. Ein-Eli, Higher, stronger, better ... a review of 5 volt cathode materials for advanced lithium-ion batteries. *Adv Energy Mater* **2**, 922–939 (2012). <https://doi.org/10.1002/aenm.201200068>
7. P.G. Bruce, B. Scrosati, J.-M. Tarascon, Nanomaterials for rechargeable lithium batteries. *Angew Chem Int Ed* **47**, 2930–2946 (2008). <https://doi.org/10.1002/anie.200702505>
8. M.R. Palacin, Recent advances in rechargeable battery materials: a chemist's perspective. *Chem Soc Rev* **38**, 2565–2575 (2009). <https://doi.org/10.1039/b820555h>



9. U. Nisar, R. Amin, R. Essehli, R.A. Shakoor, R. Kahraman, D.K. Kim, M.A. Khaleel, I. Belharouak, Extreme fast charging characteristics of zirconia modified  $\text{LiNi}_0.5\text{Mn}_1.5\text{O}_4$  cathode for lithium ion batteries. *J Power Sources* **396**, 774–781 (2018). <https://doi.org/10.1016/j.jpowsour.2018.06.065>
10. G. Jeong, Y.-U. Kim, H. Kim, Y.-J. Kim, H.-J. Sohn, Prospective materials and applications for Li secondary batteries. *Energy Environ Sci* **4**, 1986 (2011). <https://doi.org/10.1039/c0ee00831a>
11. M. Osiak, H. Geaney, E. Armstrong, C. O'Dwyer, Structuring materials for lithium-ion batteries: advancements in nanomaterial structure, composition, and defined assembly on cell performance. *J Mater Chem A* **2**, 9433 (2014). <https://doi.org/10.1039/c4ta00534a>
12. R. Amin, I. Belharouk, Part I: electronic and ionic transport properties of the ordered and disordered  $\text{LiNi}_0.5\text{Mn}_1.5\text{O}_4$  spinel cathode. *J Power Sources* **348**, 311–317 (2017). <https://doi.org/10.1016/j.jpowsour.2017.02.071>
13. R. Amin, I. Belharouak, Part-II: exchange current density and ionic diffusivity studies on the ordered and disordered spinel  $\text{LiNi}_0.5\text{Mn}_1.5\text{O}_4$  cathode. *J Power Sources* **348**, 318–325 (2017). <https://doi.org/10.1016/j.jpowsour.2017.02.070>
14. Y. Zhang, Q.Y. Huo, P.P. Du, L.Z. Wang, A.Q. Zhang, Y.H. Song, Y. Lv, G.Y. Li, Advances in new cathode material  $\text{LiFePO}_4$  for lithium-ion batteries. *Synth Met* **162**, 1315–1326 (2012). <https://doi.org/10.1016/j.synthmet.2012.04.025>
15. B. Delattre, R. Amin, J. Sander, D. Coninck, A. P. Tomsia, Y. Chiang, Impact of pore tortuosity on electrode kinetics in lithium battery electrodes : study in directionally freeze-cast. *J Electrochem Soc* **165**, 388–395 (2018). <https://doi.org/10.1149/2.1321802jes>
16. M. Okubo, E. Hosono, J. Kim, M. Enomoto, N. Kojima, T. Kudo, H. Zhou, I. Honma, Nanosize effect on high-rate Li-ion intercalation in  $\text{LiCoO}_2$  electrode. *J Am Chem Soc* **129**, 7444–7452 (2007). <https://doi.org/10.1021/ja0681927>
17. J. Geder, H.E. Hoster, A. Jossen, J. Garche, D.Y.W. Yu, Impact of active material surface area on thermal stability of  $\text{LiCoO}_2$  cathode. *J Power Sources* **257**, 286–292 (2014). <https://doi.org/10.1016/j.jpowsour.2014.01.116>
18. W. Liu, G. Hu, K. Du, Z. Peng, Y. Cao, Enhanced storage property of  $\text{LiNi}_0.8\text{Co}_0.15\text{Al}_0.05\text{O}_2$  coated with  $\text{LiCoO}_2$ . *J Power Sources* **230**, 201–206 (2013). <https://doi.org/10.1016/j.jpowsour.2012.12.065>
19. Y. Kim, J. Eom, M.G. Kim, Y.-K. Sun, C.S. Yoon, J. Cho, Comparison of structural changes in fully delithiated  $\text{Li}[\text{sub } x][\text{Ni}[\text{sub } 1\ 3]\text{Co}[\text{sub } 1\ 3]\text{Mn}[\text{sub } 1\ 3]]\text{O}[\text{sub } 2]$  and  $\text{Li}[\text{sub } x][\text{Ni}[\text{sub } 0.33]\text{Co}[\text{sub } 0.33]\text{Mn}[\text{sub } 0.30]\text{Mg}[\text{sub } 0.04]]\text{O}[\text{sub } 1.96]\text{F}[\text{sub } 0.04]$  cathodes ( $x=0$ ) upon thermal annealing. *J Electrochem Soc* **154**, A561 (2007). <https://doi.org/10.1149/1.2724761>
20. H.J. Noh, S. Youn, C.S. Yoon, Y.K. Sun, Comparison of the structural and electrochemical properties of layered  $\text{Li}[\text{Ni}_x\text{Co}_y\text{Mn}_z]\text{O}_2$  ( $x = 1/3, 0.5, 0.6, 0.7, 0.8$  and  $0.85$ ) cathode material for lithium-ion batteries. *J Power Sources* **233**, 121–130 (2013). <https://doi.org/10.1016/j.jpowsour.2013.01.063>
21. I. Belharouak, W. Lu, J. Liu, D. Vissers, K. Amine, Thermal behavior of delithiated  $\text{Li}(\text{Ni}_0.8\text{Co}_0.15\text{Al}_0.05)\text{O}_2$  and  $\text{Li}_1.1(\text{Ni}_1/3\text{Co}_1/3\text{Mn}_1/3)\text{O}_2$  powders. *J Power Sources* **174**, 905–909 (2007). <https://doi.org/10.1016/j.jpowsour.2007.06.092>
22. H.-W. Lee, P. Muralidharan, C.M. Mari, R. Ruffo, D.K. Kim, Facile synthesis and electrochemical performance of ordered  $\text{LiNi}_0.5\text{Mn}_1.5\text{O}_4$  nanorods as a high power positive electrode for rechargeable Li-ion batteries. *J Power Sources* **196**, 10712–10716 (2011). <https://doi.org/10.1016/j.jpowsour.2011.09.002>
23. T.N.L. Doan, K. Yoo, T.K.A. Hoang, P. Chen, Recent developments in synthesis of  $x\text{Li}_2\text{MnO}_3$  ( $1-x$ ) $\text{LiMO}_2$  ( $M=\text{Ni}, \text{Co}, \text{Mn}$ ) cathode powders for high-energy lithium rechargeable batteries. *Front Energy Res* **2**, 1–7 (2014). <https://doi.org/10.3389/fenrg.2014.00036>
24. M.M. Thackeray, S.-H. Kang, C.S. Johnson, J.T. Vaughey, R. Benedek, S.A. Hackney,  $\text{Li}_2\text{MnO}_3$ -stabilized  $\text{LiMO}_2$  ( $M = \text{Mn}, \text{Ni}, \text{Co}$ ) electrodes for lithium-ion batteries. *J. Mater. Chem* **17**, 3112 (2007). <https://doi.org/10.1039/b702425h>
25. X. Xiang, J. C. Knight, W. Li, A. Manthiram, Understanding the effect of Co substitution on the electrochemical properties of lithium-rich layered oxide cathodes for lithium-ion batteries. Understanding the effect of Co 3 + substitution on the electrochemical properties of lithium-rich layered oxide, (2014). doi:<https://doi.org/10.1021/jp506731v>
26. F. Wu, N. Li, Y. Su, H. Shou, L. Bao, W. Yang, L. Zhang, R. An, S. Chen, Spinel/layered heterostructured cathode material for high-capacity and high-rate li-ion batteries. *Adv. Mater* **25**, 3722–3726 (2013). <https://doi.org/10.1002/adma.201300598>
27. J.K. Noh, S. Kim, H. Kim, W. Choi, W. Chang, D. Byun, B.W. Cho, K.Y. Chung, Mechanochemical synthesis of  $\text{Li}_2\text{MnO}_3$  shell/ $\text{LiMO}_2$  ( $M = \text{Ni}, \text{Co}, \text{Mn}$ ) core-structured nanocomposites for lithium-ion batteries. *Sci. Rep.* **4**, 4847 (2014). <https://doi.org/10.1038/srep04847>
28. J. Zheng, S. Myeong, W. Cho, P. Yan, J. Xiao, C. Wang, J. Cho, J.-G. Zhang, Li- and Mn-rich cathode materials: challenges to commercialization. *Adv. Energy Mater* **7**, 1601284 (2016). <https://doi.org/10.1002/aenm.201601284>
29. F. Wu, N. Li, Y. Su, L. Zhang, L. Bao, J. Wang, L. Chen, Y. Zheng, L. Dai, J. Peng, S. Chen, Ultrathin spinel membrane-encapsulated layered lithium-rich cathode material for advanced Li-ion batteries. *Nano Lett* **14**, 3550–3555 (2014). <https://doi.org/10.1021/nl501164y>
30. Y.K. Sun, M.J. Lee, C.S. Yoon, J. Hassoun, K. Amine, B. Scrosati, The role of  $\text{AlF}_3$  coatings in improving electrochemical cycling of Li-enriched nickel-manganese oxide electrodes for Li-ion batteries. *Adv. Mater* **24**, 1192–1196 (2012). <https://doi.org/10.1002/adma.201104106>
31. L. Guo, N. Zhao, J. Li, C. He, C. Shi, E. Liu, Surface double phase network modified lithium rich layered oxides with improved rate capability for li-ion batteries. *ACS Appl. Mater. Interfaces* **7**, 391–399 (2015). <https://doi.org/10.1021/am506354e>
32. K.C. Jiang, X.L. Wu, Y.X. Yin, J.S. Lee, J. Kim, Y.G. Guo, Superior hybrid cathode material containing lithium-excess layered material and graphene for lithium-ion batteries. *ACS Appl. Mater. Interfaces* **4**, 4858–4863 (2012). <https://doi.org/10.1021/am301202a>
33. G. Kobayashi, Y. Irii, F. Matsumoto, A. Ito, Y. Ohsawa, S. Yamamoto, Y. Cui, J.Y. Son, Y. Sato, Improving cycling performance of Li-rich layered cathode materials through combination of  $\text{Al}_2\text{O}_3$ -based surface modification and stepwise precycling. *J. Power Sources* **303**, 250–256 (2016). <https://doi.org/10.1016/j.jpowsour.2015.11.014>
34. B. Song, H. Liu, Z. Liu, P. Xiao, M.O. Lai, L. Lu, High rate capability caused by surface cubic spinels in Li-rich layer-structured cathodes for Li-ion batteries. *Sci. Rep* **3**, 3094 (2013). <https://doi.org/10.1038/srep03094>
35. D.W. Shin, A. Manthiram, Surface-segregated, high-voltage spinel  $\text{LiMn}_1.5\text{Ni}_0.42\text{Ga}_0.08\text{O}_4$  cathodes with superior high-temperature cyclability for lithium-ion batteries. *Electrochem. Commun* **13**, 1213–1216 (2011). <https://doi.org/10.1016/j.elecom.2011.08.041>
36. T.-F. Yi, Y. Xie, Y.-R. Zhu, R.-S. Zhu, M.-F. Ye, High rate micron-sized niobium-doped  $\text{LiMn}_1.5\text{Ni}_0.5\text{O}_4$  as ultra high power positive-electrode material for lithium-ion batteries. *J. Power Sources* **211**, 59–65 (2012). <https://doi.org/10.1016/j.jpowsour.2012.03.095>
37. R. Alcántara, M. Jaraba, P. Lavela, J. L. Tirado, Structural and electrochemical study of new  $\text{LiNi}_{0.5}\text{TixMn}_{1.5-x}\text{O}_4$  spinel oxides

- for 5-V. *Chem Mater* **15**, 2376–2382 (2003). <https://doi.org/10.1021/cm034080s>
38. R. Alcántara, M. Jaraba, P. Lavela, J.M. Lloris, C. Pérez Vicente, J.L. Tirado, Synergistic effects of double substitution in  $\text{LiNi}[\text{sub } 0.5\text{--}y]\text{Fe}[\text{sub } y]\text{Mn}[\text{sub } 1.5]\text{O}[\text{sub } 4]$  spinel as 5 V cathode materials. *J. Electrochem. Soc* **152**, A13 (2005). <https://doi.org/10.1149/1.1827571>
  39. M. Aklalouch, J.M. Amarilla, R.M. Rojas, I. Saadoune, J.M. Rojo, Sub-micrometric  $\text{LiCr}_0.2\text{Ni}_0.4\text{Mn}_1.4\text{O}_4$  spinel as 5 V-cathode material exhibiting huge rate capability at 25 and 55 °C. *Electrochem. Commun* **12**, 548–552 (2010). <https://doi.org/10.1016/j.elecom.2010.01.040>
  40. M. Aklalouch, J.M. Amarilla, I. Saadoune, J.M. Rojo,  $\text{LiCr}_0.2\text{Ni}_0.4\text{Mn}_1.4\text{O}_4$  spinels exhibiting huge rate capability at 25 and 55 °C: analysis of the effect of the particle size. *J. Power Sources* **196**, 10222–10227 (2011). <https://doi.org/10.1016/j.jpowsour.2011.08.069>
  41. T.A. Arunkumar, A. Manthiram, Influence of chromium doping on the electrochemical performance of the 5 v spinel cathode  $\text{LiMn}_1.5\text{Ni}_0.5\text{O}_4$ . *Electrochim. Acta* **50**, 5568–5572 (2005). <https://doi.org/10.1016/j.electacta.2005.03.033>
  42. E.-S. Lee, A. Manthiram, Influence of doping on the cation ordering and charge–discharge behavior of  $\text{LiMn}_1.5\text{Ni}_0.5\text{--}x\text{MxO}_4$  (M = Cr, Fe, Co, and Ga) spinels between 5.0 and 2.0 V. *J. Mater. Chem. A* **1**, 3118 (2013). <https://doi.org/10.1039/c2ta01171a>
  43. J. Liu, A. Manthiram, Understanding the improved electrochemical performances of Fe-substituted 5V spinel cathode  $\text{LiMn}_1.5\text{Ni}_0.5\text{O}_4$ . *J. Phys. Chem. C* **113**, 15073–15079 (2009). <https://doi.org/10.1021/jp904276t>
  44. K.R. Chemelewski, D.W. Shin, W. Li, A. Manthiram, Octahedral and truncated high-voltage spinel cathodes: the role of morphology and surface planes in electrochemical properties. *J. Mater. Chem. A* **1**, 3347 (2013). <https://doi.org/10.1039/c3ta00682d>
  45. J.-S. Kim, K. Kim, W. Cho, W.H. Shin, R. Kanno, J.W. Choi, A truncated manganese spinel cathode for excellent power and lifetime in lithium-ion batteries. *Nano Lett* **12**, 6358–6365 (2012). <https://doi.org/10.1021/nl303619s>
  46. X. Zhang, F. Cheng, J. Yang, J. Chen,  $\text{LiNi}_{0.5}\text{Mn}_{1.5}\text{O}_4$  porous nanorods as high-rate and long-life cathodes for Li-ion batteries. *Nano Lett* **13**, 2822–5 (2013). <https://doi.org/10.1021/nl401072x>
  47. Y. Fan, J. Wang, Z. Tang, W. He, J. Zhang, Effects of the nanostructured  $\text{SiO}_2$  coating on the performance of  $\text{LiNi}_0.5\text{Mn}_1.5\text{O}_4$  cathode materials for high-voltage Li-ion batteries. *Electrochim. Acta* **52**, 3870–3875 (2007). <https://doi.org/10.1016/j.electacta.2006.10.063>
  48. J. Li, Y. Zhang, J. Li, L. Wang, X. He, J. Gao,  $\text{AlF}_3$  coating of  $\text{LiNi}_0.5\text{Mn}_1.5\text{O}_4$  for high-performance Li-ion batteries. *Ionics (Kiel)* **17**, 671–675 (2011). <https://doi.org/10.1007/s11581-011-0617-4>
  49. J. Liu, A. Manthiram, Understanding the improvement in the electrochemical properties of surface modified 5 V  $\text{LiMn}_1.42\text{Ni}_0.42\text{Co}_0.16\text{O}_4$  spinel cathodes in lithium-ion cells. *Chem. Mater* **21**, 1695–1707 (2009). <https://doi.org/10.1021/cm9000043>
  50. H.M. Wu, I. Belharouak, A. Abouimrane, Y.K. Sun, K. Amine, Surface modification of  $\text{LiNi}_0.5\text{Mn}_1.5\text{O}_4$  by  $\text{ZrP}_2\text{O}_7$  and  $\text{ZrO}_2$  for lithium-ion batteries. *J. Power Sources* **195**, 2909–2913 (2010). <https://doi.org/10.1016/j.jpowsour.2009.11.029>
  51. M.-J. Lee, E. Lho, P. Oh, Y. Son, J. Cho, Simultaneous surface modification method for  $0.4\text{Li}_2\text{MnO}_3 \cdot 0.6\text{LiNi}_{1/3}\text{Co}_{1/3}\text{Mn}_{1/3}\text{O}_2$  cathode material for lithium ion batteries: acid treatment and  $\text{LiCoPO}_4$  coating. *Nano Res* **10**(12), 4210–20 (2017). <https://doi.org/10.1007/s12274-017-1662-8>
  52. M. Aklalouch, J.M. Amarilla, R.M. Rojas, I. Saadoune, J.M. Rojo, Sub-micrometric  $\text{LiCr}_0.2\text{Ni}_0.4\text{Mn}_1.4\text{O}_4$  spinel as 5V-cathode material exhibiting huge rate capability at 25 and 55°C. *Electrochem. Commun* **12**, 548–552 (2010). <https://doi.org/10.1016/j.elecom.2010.01.040>
  53. J. Liu, A. Manthiram, Understanding the improved electrochemical performances of Fe-substituted 5 V spinel cathode  $\text{LiMn}_1.5\text{Ni}_0.5\text{O}_4$ . *J. Phys. Chem. C* **113**, 15073–15079 (2009). <https://doi.org/10.1021/jp904276t>
  54. D.W. Shin, A. Manthiram, Surface-segregated, high-voltage spinel  $\text{LiMn}_1.5\text{Ni}_0.42\text{Ga}_0.08\text{O}_4$  cathodes with superior high-temperature cyclability for lithium-ion batteries. *Electrochem. Commun* **13**, 1213–1216 (2011). <https://doi.org/10.1016/j.elecom.2011.08.041>
  55. R. Alcántara, M. Jaraba, P. Lavela, J. L. Tirado, Structural and electrochemical study of new  $\text{LiNi}_{0.5}\text{TixMn}_{1.5-x}\text{O}_4$  spinel oxides for 5-V cathode materials. *Chem Mater* **15**(12), 2376–82 (2003). <https://doi.org/10.1021/cm034080s>
  56. M. Aklalouch, J.M. Amarilla, R.M. Rojas, I. Saadoune, J.M. Rojo, Chromium doping as a new approach to improve the cycling performance at high temperature of 5 V  $\text{LiNi}_0.5\text{Mn}_1.5\text{O}_4$ -based positive electrode. *J. Power Sources* **185**, 501–511 (2008). <https://doi.org/10.1016/j.jpowsour.2008.06.074>
  57. W.K. Pang, H.F. Lin, V.K. Peterson, C.Z. Lu, C.E. Liu, S.C. Liao, J.M. Chen, Effects of fluorine and chromium doping on the performance of lithium-rich  $\text{Li}_{1+x}\text{MO}_2$  (M = Ni, Mn, Co) positive electrodes. *Chem. Mater* **29**, 10299–10311 (2017). <https://doi.org/10.1021/acs.chemmater.7b02930>
  58. R.M. Rojas, K. Petrov, G. Avdeev, J.M. Amarilla, L. Pascual, J.M. Rojo, High-temperature thermal behaviour of Cr-doped  $\text{LiMn}_2\text{O}_4$  spinels synthesized by the sucrose-aided combustion method. *J. Therm. Anal. Calorim* **90**, 67–72 (2007). <https://doi.org/10.1007/s10973-007-8477-x>
  59. K.A. Jarvis, Z. Deng, L.F. Allard, A. Manthiram, P.J. Ferreira, Atomic structure of a lithium-rich layered oxide material for lithium-ion batteries: Evidence of a solid solution. *Chem. Mater* **23**, 3614–3621 (2011). <https://doi.org/10.1021/cm200831c>
  60. S. Shi, T. Wang, M. Cao, J. Wang, M. Zhao, G. Yang, Rapid self-assembly spherical  $\text{Li}_1.2\text{Mn}_0.56\text{Ni}_0.16\text{Co}_0.08\text{O}_2$  with improved performances by microwave hydrothermal method as cathode for lithium-ion batteries. *ACS Appl. Mater. Interfaces* **8**, 11476–11487 (2016). <https://doi.org/10.1021/acsami.6b01683>
  61. Y. Gao, P. Xu, F. Chen, C. Ding, L. Chen, D. Li, Facile synthesis of nanostructured  $\text{MoO}_3$  coated  $\text{Li}_1.2\text{Mn}_0.56\text{Ni}_0.16\text{Co}_0.08\text{O}_2$  materials with good electrochemical properties. *RSC Adv* **6**, 113275–113282 (2016). <https://doi.org/10.1039/C6RA21637D>
  62. J.M. Kim, H.T. Chung, The first cycle characteristics of  $\text{Li}[\text{Ni}_{1/3}\text{Co}_{1/3}\text{Mn}_{1/3}]\text{O}_2$  charged up to 4.7 V. *Electrochim. Acta* **49**, 937–944 (2004). <https://doi.org/10.1016/j.electacta.2003.10.005>
  63. T. Ohzuku, Y. Makimura, Layered lithium insertion material of  $\text{LiNi}_{1/2}\text{Mn}_{1/2}\text{O}_2$ : a possible alternative to  $\text{LiCoO}_2$  for advanced lithium-ion batteries. *Chem. Lett* **2**, 744–745 (2001). <https://doi.org/10.1246/cl.2001.744>
  64. B. J. Hwang, Y. W. Tsai, D. Carlier, G. Ceder, A combined computational/experimental study on  $\text{LiNi}_{1/3}\text{Co}_{1/3}\text{Mn}_{1/3}\text{O}_2$ . *Chem Mater* **15**(19), 3676–82 (2003). <https://doi.org/10.1021/cm030299v>
  65. Y. Koyama, I. Tanaka, H. Adachi, Y. Makimura, T. Ohzuku, Crystal and electronic structures of superstructural  $\text{Li}_{1-x}[\text{Co}_{1/3}\text{Ni}_{1/3}\text{Mn}_{1/3}]\text{O}_2$  ( $0 \leq x \leq 1$ ). *J. Power Sources* **119–121**, 644–648 (2003). [https://doi.org/10.1016/S0378-7753\(03\)00194-0](https://doi.org/10.1016/S0378-7753(03)00194-0)